Materials Letters 149 (2015) 66–69

Contents lists available at ScienceDirect

Materials Letters

journal homepage: www.elsevier.com/locate/matlet

Enhanced field electron emission of flower-like zinc oxide on zinc oxide nanorods grown on carbon nanotubes

A.B. Suriani [a,b,*], R.N. Safitri [a,b], A. Mohamed [a,c], S. Alfarisa [a,b], I.M. Isa [a,c], A. Kamari [a,c], N. Hashim [a,c], M.K. Ahmad [d], M.F. Malek [e], M. Rusop [e]

[a] Nanotechnology Research Centre, Faculty of Science and Mathematics, Universiti Pendidikan Sultan Idris, 35900 Tanjung Malim, Perak, Malaysia
[b] Department of Physics, Faculty of Science and Mathematics, Universiti Pendidikan Sultan Idris, 35900 Tanjung Malim, Perak, Malaysia
[c] Department of Chemistry, Faculty of Science and Mathematics, Universiti Pendidikan Sultan Idris, 35900 Tanjung Malim, Perak, Malaysia
[d] Microelectronic and Nanotechnology – Shamsuddin Research Centre (MiNT-SRC), Faculty of Electrical and Electronic Engineering, Universiti Tun Hussein Onn Malaysia, 86400 Parit Raja, Batu Pahat, Johor, Malaysia
[e] NANO-ElecTronic Centre, Faculty of Electrical Engineering, Universiti Teknologi MARA, 40450 Shah Alam, Malaysia

ARTICLE INFO

Article history:
Received 21 January 2015
Accepted 23 February 2015
Available online 3 March 2015

Keywords:
Zinc oxide
Carbon nanotubes
Chemical vapour deposition
Electron microscopy

ABSTRACT

For the first time, zinc oxide (ZnO) nanoflowers on ZnO nanorods were produced on carbon nanotubes (CNTs) synthesised from waste cooking palm oil precursor. First, CNTs were grown using a thermal chemical vapour deposition method. Next, ZnO nanostructures were deposited using the sonicated sol–gel immersion method and the prepared samples were characterised using electron microscopy, micro-Raman spectroscopy and X-ray diffraction. The field electron emission properties of the samples indicated that the ZnO nanoflowers grown on the CNTs had better emission performances than the pristine aligned ZnO nanorods. The resulting CNTs/ZnO nanocomposite had reasonable turn-on and threshold fields of 4.6 and 6.7 V/μm, which corresponded with the electric fields required to create current densities of 1.0 μA/cm^2 and 0.1 mA/cm ^{2}, respectively. This study shows the important roles of CNTs in ZnO nanoflowers growth and the abilities of CNTs to enhance ZnO emission properties.

1. Introduction

The study of field electron emissions (FEE) is interesting due to its wide range of applications, such as in flat panel displays and high brightness electron sources [1]. Generally, the material used as the electron emitter in this process may be damaged due to current-induced heating [2]. Therefore, the chosen emitter should have high mechanical and thermal strengths.

Generally, ZnO nanomaterials have good emissions properties due to their excellent structures, which can be tuned into various morphologies with high chemical, thermal and mechanical stabilities [3,4]. However, the moderate turn-on field of ZnO nanostructures (9.1 V/μm at a current density of 10^{-3} μm/cm^2) [5] and limitations in their lengths (not more than 1–20 μm) [6] have impeded their application in FEE devices. Numerous modifications of ZnO nanostructures have been conducted to enhance FEE properties, such as density controlling and oxygen treatments [7], length controlling treatments [8] and composition alterations using amorphous carbon [9]. However, these approaches are not simple and are expensive because they require high temperature and pressure during the fabrication process.

On the other hand, carbon nanotubes (CNTs) are good emitters for FEE devices due to their high aspect ratios, chemical stability, thermal strength and high mechanical strength. However, their low resistance to ambient oxygen results in the degradation of the CNTs emitter [10]. Combining CNTs and ZnO into nanocomposites significantly affects the electron emission performances of composite materials [11]. Numerous synthesis methods, including simultaneous and sequential processes, have been conducted to fabricate CNTs/ZnO nanocomposites. The simultaneous deposition of CNTs/ZnO nanocomposites via chemical vapour deposition (CVD) has been reported [12]. Although the simultaneous process is generally a simple approach, controlling and diversifying the morphologies of the CNTs/ZnO nanocomposites was difficult, and mainly ZnO nanoparticles were deposited. The preparation of CNTs/ZnO using a sequence process could control the morphologies of the CNTs/ZnO. Previously, the formation of cone and hexagonal-type ZnO nanorods (ZNRs) on CNTs enhanced the FEE properties of CNTs/ZnO nanocomposites [13].

In this study, for the first time ZnO nanoflowers (ZNFs) were successfully grown on ZNRs in the presence of CNTs, and this

* Corresponding author at: Department of Physics, Faculty of Science and Mathematics, Universiti Pendidikan Sultan Idris, 35900 Tanjung Malim, Perak, Malaysia. Tel.: +60 192117002; fax: +60 1548117296.
E-mail address: absuriani@yahoo.com (A.B. Suriani).

http://dx.doi.org/10.1016/j.matlet.2015.02.115
0167-577X/

nanocomposite material exhibited an enhanced FEE performance. The synthesis of ZnO nanostructure on CNTs was achieved using a low-cost sonicated sol–gel immersion method. The CNTs were initially synthesised from a natural precursor, waste cooking palm oil (WCPO), using the thermal CVD (TCVD) method. The use of such waste material highlights for both environmental and economic benefits. A proposed growth mechanism for the CNTs/ZnO nanocomposite is presented.

2. Experimental

The growth of ZnO nanostructures on CNTs was performed in three steps. First, the CNTs were synthesised on $2 \times 2\ cm^2$ Si substrates from the WCPO precursor in a 2-stage TCVD furnace (similar to the experimental set-up reported in [14]). Next, magnesium zinc oxide (MgZnO) seeded catalyst was coated on the as-grown CNTs using spin coating. Then, ZnO nanostructures were grown on the MgZnO-coated CNTs using an immersion method. Details of the coating and immersion processes were previously reported in [15]. Finally, the CNTs/ZnO samples were collected and rinsed with deionised water before annealing at 500 °C for 1 h.

Field emission scanning electron microscopy (FESEM-QUANTA 450 FEG), high-resolution transmission electron microscopy (HRTEM-JOEL-2100), micro-Raman spectroscopy (Renishaw InVia microRaman System) and X-ray diffraction (XRD) (PANalytical X'pert Pro XRD) were used to determine the morphologies of the

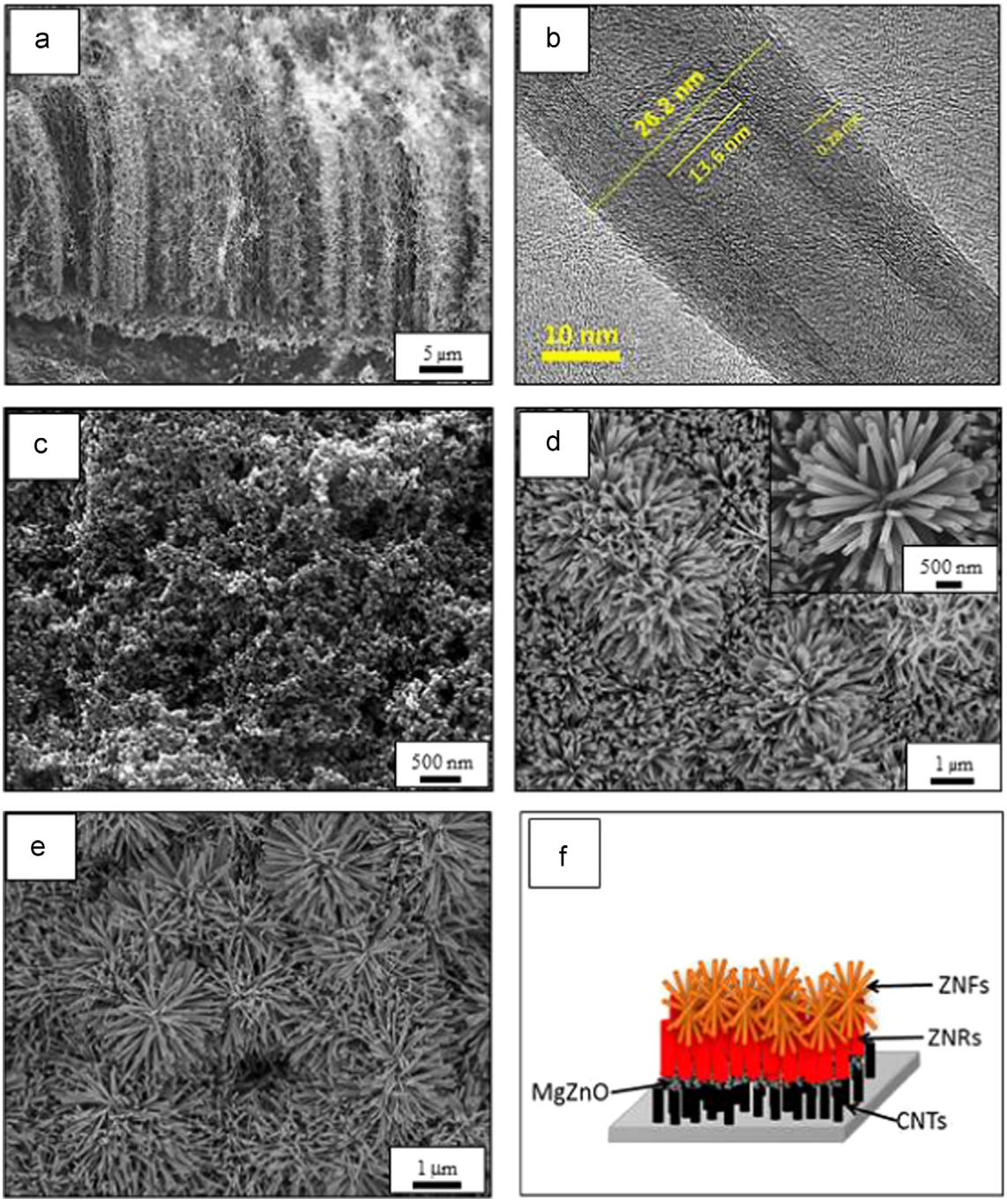

Fig. 1. (a) CNTs on Si substrate, (b) HRTEM of CNTs, (c) MgZnO-coated CNTs, (d) and (e) growth of ZNFs on ZNRs and (f) illustration of CNTs/ZnO configuration.

samples and to identify their phases. Ultimately, the FEE measurements were conducted to investigate the emissions properties of the samples (see Supplementary material for details regarding the FEE measurement set-up).

3. Results and discussion

The FESEM images of the prepared samples are shown in Fig. 1. Vertically aligned CNTs were grown with diameters of 20–40 nm and lengths of 15.5–18.2 μm (Fig. 1(a)). One critical observation using HRTEM analysis (Fig. 1(b)) revealed that the multi-walled CNTs consisted of approximately 20 layers. The inner diameter of the tube was 13.6nm, and the distance between the walls was 0.28 nm. The MgZnO nanostructures grew unevenly on the CNTs, as shown in Fig. 1(c). The uneven surfaces of the CNTs potentially contributed to the uneven growth of MgZnO, in contrast with the deposition of MgZnO on a bare Si substrate (Fig. S1) (further explanations are provided in Supplementary material). The subsequent growth of ZNFs on the initially produced ZNRs is shown in Fig. 1(d) and (e). The ZNFs constructed of rod structures had diameters of 46.9–82.7 nm, while the average diameter of the aligned ZNRs was 128 nm. The agglomeration of the MgZnO nanoparticles likely contributed to the larger diameters of the ZNRs. The sample configuration is shown in Fig. 1(f).

The micro-Raman spectra of the CNTs/ZnO sample (Fig. S2) show the characteristic peaks of CNTs and ZnO (analysis details are provided in Supplementary material). The I_D/I_G ratio of the CNTs in the composite sample was larger (0.86) than the pristine CNTs (0.69). This result indicated that the defect level of CNTs was higher after the deposition of ZnO. This was supported by the XRD analysis (Fig. S3) where a broader peak for the carbon phase in the sample indicated that the CNTs had moderate crystallinity after combining with ZnO (see Supplementary material).

Curves of the current density (J) vs the electric field (E) from FEE measurements of the pristine ZnO and CNTs/ZnO samples are shown in Fig. 2(a). The turn-on and threshold fields of the CNTs/ZnO sample were 4.6 and 6.7 V/μm, which corresponded with the electric field required to generate current densities of 1.0m, whi^2 and 0.1 mA/cm^2, respectively. The field enhancement factor (β) determined from the slope of the Fowler–Nordheim (FN) plot (Fig. 2(b)) was 1217. Compared with the pristine ZnO (turn-on 6.9 V/μm), the CNTs/ZnO sample showed better FEE performances. Moreover, the threshold field of pristine ZnO could not be determined because the maximum current density of the sample was only 1.1 μA/cm^2 at electric field of 7.0 V/μm. The presence of highly conductive CNTs provided more electrons in the sample, decreased the work function and generated better ohmic contact [16]. Therefore, lower turn-on and threshold fields and higher emission currents were observed in the CNTs/ZnO nanocomposite sample. In addition, the formation of ZNFs reduced the screening effect of the densely aligned ZNRs, which is beneficial for the electron emission process.

The mechanisms of ZNFs growth on ZNRs that were grown on CNTs are proposed in Fig. 3. The CNTs/MgZnO-coated substrate was immersed in a ZnO solution by allowing it to float while facing downward, as shown in Fig. 3(a). Next, the zinc-hexamethylenetetramine (Zn-HMT) complex interacted with the MgZnO and CNTs (Fig. 3(b)). The HMT immediately attached to the non-polar facets of ZnO, which resulted in hexagonal ZnO and initially led to the formation of ZNRs (Fig. 3(c)). The typical reactions that occur during the formation of ZNRs have been reported [17]. The OH^- ions were believed to react with the CNTs (Fig. 3(d)), which reduced the supply of OH^- during the formation of the ZNRs. Here, we suggest the chemical reaction occurred between OH^- and CNTs:

$$Zn^{2+} + 4OH^- + 2C \rightleftarrows ZnO + CO_2 + C + H_2O + H_2 + 2e^- \quad (1)$$

Due to the interactions between OH^- and CNTs, slow nucleation and agglomeration of ZnO nuclei occurred on the surfaces of the ZNRs. Consequently, multiple growth unit orientations were produced, resulting in the growth of ZNFs on the ZNRs [18]. Therefore, the presence of CNTs is important for the formation of flower-like ZnO, and CO_2 and H_2 gases were released during the reaction.

4. Conclusions

Flower-like ZnO was successfully synthesised on ZNRs on CNTs by using the sonicated sol–gel immersion method. The I_D/I_G ratio of the CNTs increased during ZnO synthesis, which indicated that the as-grown CNTs were affected by the ZnO deposition and annealing processes. Slow nucleation resulted from the interactions between the ZnO precursor (OH^-) and the CNTs resulted in the formation of flower-like ZnO on the ZNRs. Therefore, the presence of CNTs is important for the formation of flower-like ZnO. This structure reduces the screening effects of ZNRs and serves as a good electron emitter with a low turn-on field of 4.6 V/μm and a high β value of 1217.

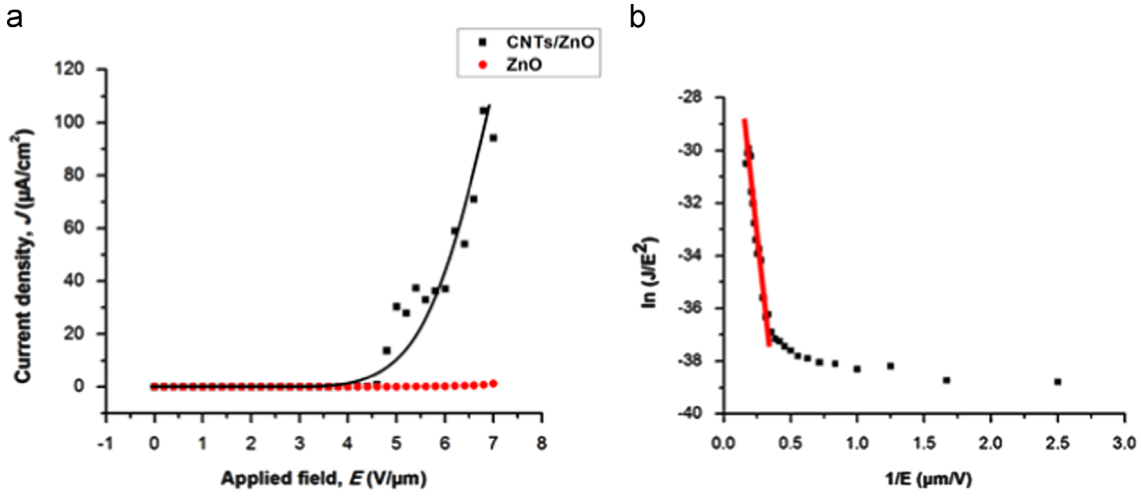

Fig. 2. (a) J–E curves of pristine ZnO and CNTs/ZnO and (b) FN plot of CNTs/ZnO sample.

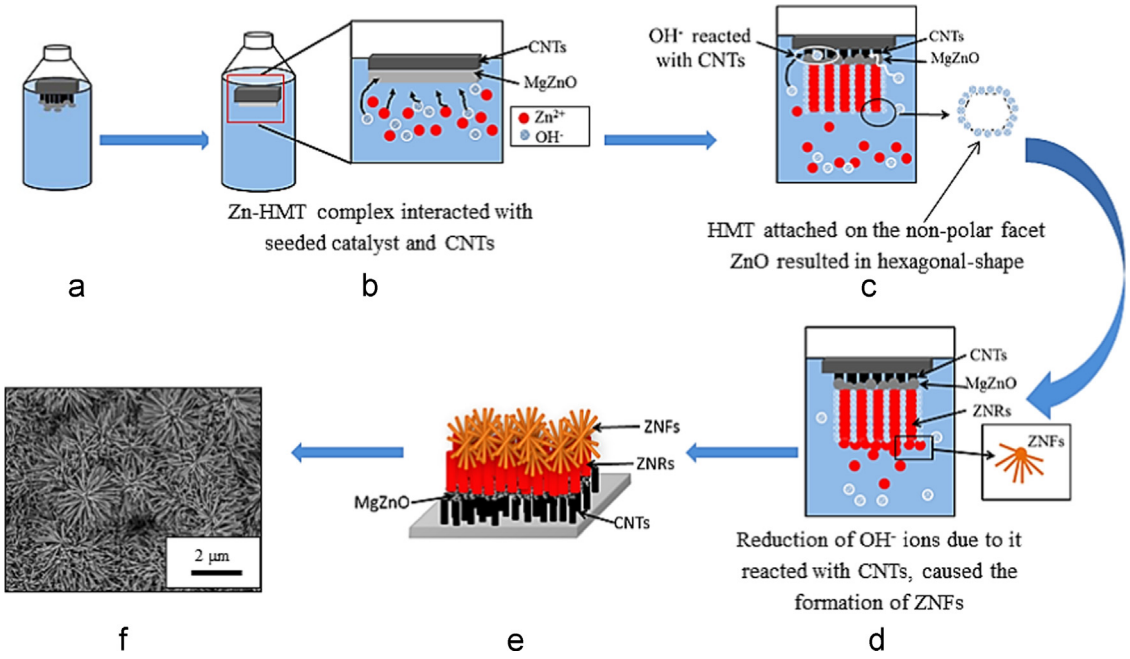

Fig. 3. Schematic diagram of the possible growth mechanism of ZNFs on ZNRs by the presence of CNTs.

Acknowledgements

The authors acknowledge the RACE (2012-0147-102-62) and PRGS (2013-0097-102-32) grants and UPSI for supporting this work.

Appendix A. Supporting information

Supplementary data associated with this article can be found in the online version at http://dx.doi.org/10.1016/j.matlet.2015.02.115.

References

[1] Ling-min Y, Xin-hui F, Li-jun Q, Wen Y. Appl Surf Sci 2011;257(15):6332–5.
[2] Hirayama H, Kawamoto Y, Ohshima Y, Takayanagi K. Appl Phys Lett 2001;79:1169–71.
[3] Malek MF, Mamat MH, Khusaimi Z, Sahdan MZ, Musa MZ, Zainun AR, et al. J Alloy Compd 2014;582:2–21.
[4] Rouhi J, Alimanesh M, Mahmud S, Dalvand RA, Raymond CH, Rusop M. Mater Lett 2014;125:147–50.
[5] Mosquera E, Bernal J, Zarate RA, Mendoza F, Katiyar, Morell G. Mater Lett 2013;93:326–9.
[6] Ok JG, Tawfick SH, Juggernauth KA, Sun K, Zhang Y, Hart AJ. Adv Funct Mater 2010;20:2470–80.
[7] Ma LA, Guo TL. Ceram Int 2013;39:6923–9.
[8] Singh J, Patil SS, More MA, Joag DS, Tiwari RS, Srivastava ON. Appl Surf Sci 2010;256:6157–63.
[9] Nawn D, Banerjee D, Chattopadhyay. Diam Relat Mater 2013;34:50–9.
[10] Ham H, Shen G, Cho JH, Lee TJ, Seo SH, Lee CJ. Chem Phys Lett 2005;404:69–73.
[11] Yan X, Tay BK, Miele P. Carbon 2008;46:753–8.
[12] Klanwan J, Akrapattangkul N, Pavarajarn Seto T, Otani Y, Charinpanitkul T. Mater Lett 2010;64:80–2.
[13] Seo M, Jung Y, Lim D, Cho D, Jeong Y. Mater Lett 2013;92:177–80.
[14] Suriani AB, Md Nor R, Rusop M. J Ceram Soc Jpn 2010;118(1382):963–8.
[15] Salina M, Suriani AB, Rusop M. Trans Electron Mater 2012;13(2):64–8.
[16] Yu LM, Zhu CC. Appl Surf Sci 2009;255(20):8359–62.
[17] Mamat MH, Khusaimi Z, Zahidi MM, Bakar SA, Siran YM, Rejab SAM, et al. Jpn J Appl Phys 2011;50(6):1–6.
[18] Baruah S, Dutta J. J Sol–Gel Sci Technol 2009;50(3):456–64.